ADVANCED FUNCTIONAL MATERIALS
www.afm-journal.de



# 3D Stack Integrated Triboelectric Nanogenerator for Harvesting Vibration Energy

*Weiqing Yang, Jun Chen, Qingshen Jing, Jin Yang, Xiaonan Wen, Yuanjie Su, Guang Zhu, Peng Bai, and Zhong Lin Wang**

**The applications of a single-layer triboelectric nanogenerator (TENG) may be challenged by its lower output current, and a possible solution is to use three-dimensional (3D) integrated multilayered TENGs. However, the most important point is to synchronize the outputs of all the TENGs so that the instantaneous output power can be maximized. Here, a multi-layered stacked TENG is reported as a cost-effective, simple, and robust approach for harvesting ambient vibration energy. With superior synchronization, the 3D-TENG produces a short-circuit current as high as 1.14 mA, and an open-circuit voltage up to 303 V with a remarkable peak power density of 104.6 W m$^{-2}$. As a direct power source, it is capable of simultaneously lighting up 20 spot lights (0.6 W ea.) as well as a white G16 globe light. Furthermore, compared with the state-of-the-art vibration energy harvesters, the 3D-TENG has an extremely wide working bandwidth up to 36 Hz in low frequency range. In addition, with specific dimensional design, the 3D-TENG is successfully equipped inside a ball with a diameter of 3 inches, using which 32 commercial LEDs are simultaneously lighted up via hand shaking, exhibiting great potential of scavenging the abundant but wasted kinetic energy when people play basketball, football, baseball, and so on.**

## 1. Introduction

Tremendous amounts of vibration energy extensively exist in ambient environment, such as ocean waves, vehicle systems, highway, bridge and building vibration. And the majority of the ambient vibrations are dominant at very low frequencies.[1,2] Nowadays, harvesting vibration energy mainly focuses on piezoelectric,[3–6] electrostatic,[7–9] magnetostrictive effect,[10–12] aiming at building up self-powdered systems to drive small electronics.[11,12,14]

Recently, triboelectric nanogenerator,[13–22] a conjunction use of the universally known contact electrification effect[23–28] and electrostatic induction, has been proved to be a cost-effective and robust approach for harvesting ambient mechanical energy. A challenge to TENG is its relatively low output current but a high voltage output. Recently, we developed an integrated rhombic gridding based TENG as an effective solution to this problem through structurally multiplied unit cells connected in parallel.[16] However, since the current output of each unit is a pulse at the moment when two contact surfaces approaching and separating,[13–22] in such short period of time, these units are impossible to operate in a synchronized manner to maximize the power output. Here, we present a 3D stack integrated TENG that is designed to rationally solve this problem. With polytetrafluoroethylene (PTFE) nanowire arrays as surface modification, the open-circuit voltage ($V_{oc}$) and short-circuit current ($I_{sc}$) of the TENG reach up to 303 V and 1.14 mA, respectively, corresponding to a remarkable peak power density of 104.6 W m$^{-2}$. Moreover, the 3D-TENG shows an extremely wide working bandwidth up to 36 Hz in low vibration frequency range. The generated power by the TENG is high enough to simultaneously light up more than 20 spot lights (0.6 W ea.) as well as a white globe light, which unambiguously demonstrated the capability of the 3D-TENG acting as a sustainable power source for mobile electronics. In addition, with specific dimensional design, we integrated a 3D-TENG inside a ball with a diameter of 3 inches, the generated power by hand shaking simultaneously lighted up 32 commercial LEDs, which greatly demonstrated its capability of harvesting kinetic energy when people play various kinds of ball sports. And also, a large amount of these self-powered balls can also be woven into webs for ocean wave energy harvesting, which can be potentially applied to large-scale energy generation.

## 2. Design and Analysis

The 3D-TENG has a multilayered structure with acrylic as supporting substrates, as schematically shown in **Figure 1**a.

Dr. W. Yang,[+] J. Chen,[+] Q. Jing, Dr. J. Yang, X. Wen, Y. Su, Dr. G. Zhu, P. Bai, Prof. Z. L. Wang
School of Materials Science and Engineering
Georgia Institute of Technology
Atlanta, Georgia 30332–0245, USA
E-mail: zlwang@gatech.edu
Dr. W. Yang, Y. Su
State Key Laboratory of Electronic Thin films and Integrated Devices
University of Electronic Science and Technology of China
Chengdu 610054, China
Prof. Z. L. Wang
Beijing Institute of Nanoenergy and Nanosystems
Chinese Academy of Sciences
Beijing 100083, China
[+]W.Y. and J.C. contributed equally to this work.

DOI: 10.1002/adfm.201304211

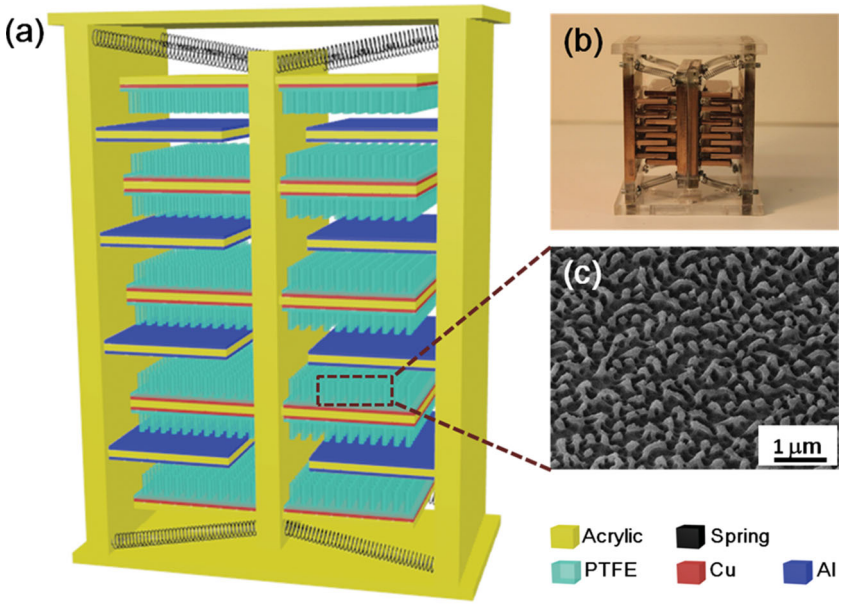


**Figure 1.** Three-dimensional triboelectric nanogenerator. a) Schematic of a 3D-TENG. b) SEM image of nanopores on aluminum electrode. c) A photograph of the as fabricated 3D-TENG.

Acrylic was selected as the structural material due to its decent strength, light weight, good machinability and low cost. A photograph of an as-fabricated TENG is shown in Figure 1b, in which, the total number of the unit cells can be expressed as:

$$N_{\text{total}} = 4n \tag{1}$$

where $n$ is the number of pinned fingers of a TENG and its definition is illustrated in Figure S1 (Supporting Information). Eight identical springs were employed to bridge the moveable and pinned fingers. All fingers were made from acrylic sheets with a thickness of 3 mm and parallel to each other with identical but tuneable gap distance. The thickness of acrylic sheets is large enough to prevent the mutual charges influences among the unit cells.[16,22] Moreover, all the unit cells are electrically connected in parallel, which is illustrated in Figure S2 (Supporting Information). Aluminium thin films were deposited onto both sides of the pinned fingers, which played dual roles of a contact electrode and a contact surface. A layer of polytetrafluoroethylene (PTFE) film was adhered to the both sides of the movable fingers with deposited copper as another electrode. PTFE nanowires arrays were created on the exposed PTFE surface by a top-down method through reactive ion etching. SEM image of the PTFE nanowires is displayed in Figure 1c. Additionally, to promote the triboelectrification and to increase the effective contact area between the two contacting surfaces, PTFE nanowires are created as surface modifications, which greatly increases the triboelectric charges and thus the overall electrical output. Detailed fabrication specifications are presented in the Experimental Section.

Once the 3D-TENG is being triggered by an external vibrational source, a periodic of electricity generation process is illustrated in **Figure 2**. A periodic contact and separation between two materials with opposite triboelectric polarities alternatingly drives induced electrons through external circuit due to

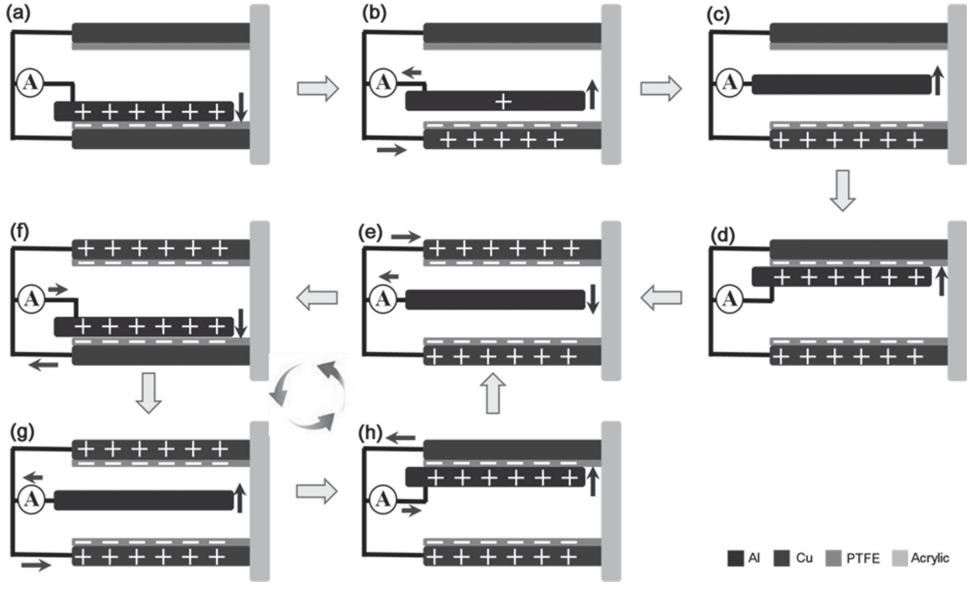


**Figure 2.** A sketch illustrating the working principle of the 3D-TENG. a) The positive and negative triboelectric charges are respectively generated on the aluminum side and the PTFE side due to contact electrification. b) The applied external force causes a separation. Electric potential difference drives electrons from the back electrode to contact electrode, screening the induced charges. c) A pinned finger arrived at the middle position between two adjacent movable fingers. All of the electrons in the back electrode are almost driven to the contact electrode. d) The pinned fingers keeps relatively moving up due to the inertia and contacts with upper movable fingers. e–h) A complete cycle of electricity generation process for the 3D-TENG.

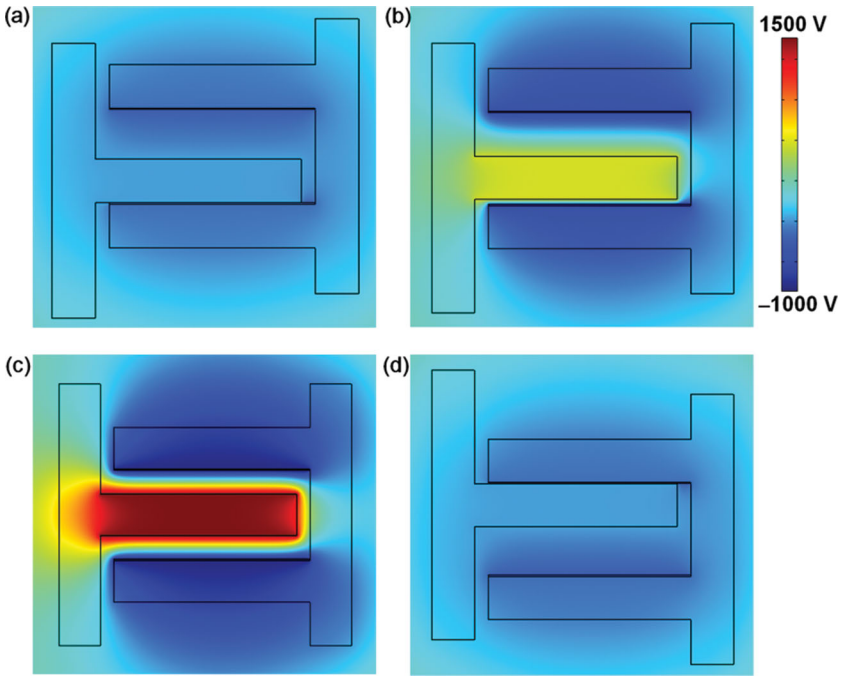


**Figure 3.** Finite element simulation of the periodic potential change between the two electrodes upon vertical contact and separation, showing the driving force for the back-and-forth charge flow generated by the TENG. A cycle is generally divided into four states: a) Initial contact. b) Separation after contact. c) A pinned finger arrives at the middle position between two adjacent movable fingers. d) The pinned finger arrives and contacts with the upper movable finger.

the coupling of triboelectric effect and electrostatic induction effect.[13–22] At the original position, all pinned fingers are stationary and stay in the middle of two adjacent movable fingers. Due to the applied external vibration, the pinner fingers will be brought to contact with the moving fingers. According to the triboelectric series,[29] electrons are injected from aluminium electrode into PTFE,[13–16,24,30–32] resulting in negative charges at the surface of the PTFE film and positive charges at the aluminium electrode, as demonstrated in Figure 2a. Subsequently, external vibration induced relative motion will cause a separation between the pinned and movable fingers, producing an electric potential difference across the electrodes, which drives most electrons from back electrode to the contact electrode through the external circuit in an ultrashort period of time, screening the positive triboelectric charges on the back electrode, as shown in Figure 2b. When the pinned fingers reach the middle position of two adjacent movable fingers, the positive triboelectric charges are almost neutralized by the inductive electrons (Figure 2c). After the middle point, continuous relative motion will bring about a second contact and thus triboelectrification between the moving and pinned fingers, as demonstrated in Figure 2d. Owing to the periodicity of applied vibration motion, the pinned fingers will separate from the movable fingers a second time, and thus another electric potential difference is emerged and maximized when the pinned fingers come back to the middle point (Figure 2e). In a cycle of vibration motion, two contacts and two separations will occur, corresponding to four current pulses in the external circuit. And a complete cycle of electricity generation process for the 3D-TENG is illustrated in Figure 2e–h.

Additionally, in order to consolidate the working principle of the 3D-TENG, by virtue of COMSOL, we took a further step to simulate the periodic potential change between the two electrodes upon vertical contact and separation, as demonstrated in **Figure 3**a–d. And the continuous variation of the potential distribution is visualized in Supporting Information Movie 1.

## 3. Results and Discussion

In an as-fabricated 3D-TENG, all of the fingers are not only structurally parallel to each other, but also electrically connected in parallel. To evaluate the TENG's performance for harvesting vibration energy, an electrodynamic shaker (Labworks Inc.) that provides sinusoidal wave was employed as an external vibration source with tunable frequency and amplitude. The bottom substrate of the 3D-TENG with $n = 5$ was anchored on the shaker. At a fixed vibration amplitude, the reliance of electric output on the input vibration frequency is presented in **Figure 4**a,b, which was measured with input frequency varying from 2 Hz to 54 Hz, indicating that 40 Hz is the resonance frequency of the TENG. Compared to the state-of-the-art vibration energy harvesters that are based on nonlinear and topology variation,[33–35] it has a wide working bandwidth of 36 Hz in low frequency range (Figure S3, Supporting Information). As demonstrated in Figure 4c,d, the open-circuit voltage ($V_{oc}$) and short-circuit current ($I_{sc}$) are respectively as high as 303 V and 1.14 mA at the resonance vibration frequency of 40 Hz. Insets are the enlarged view of the output signals in one cycle of vibration. It is worth noting that $I_{sc}$ has an alternating behavior with asymmetrical amplitudes. And it is found that, the larger peaks correspond to the process in which the two fingers approach each other, while the smaller ones are generated as the two fingers move apart after contacting. Given the same amount of charges ($\Delta Q$) transported back and forth, a faster approaching is expected to produce larger current peaks ($I_{sc} = \Delta Q/\Delta t$) than that during the slower separation.

Additionally, we take a further step to make a systematical study of the reliance of current output on the design parameters, such as, the number of pinned fingers $n$, effective contact area $\Delta S$ and gap distance between the two adjacent fingers $\Delta d$.

Theoretically, the short-circuit current of the 3D-TENG can be expressed as (see Figure S4 and other Supporting Information for detailed derivation of the analytical model):[16]

$$I_{sc} = \frac{\sigma s d_0 v}{\varepsilon_r \left[ d + \frac{d_0}{\varepsilon_r} \right]^2} \quad (2)$$

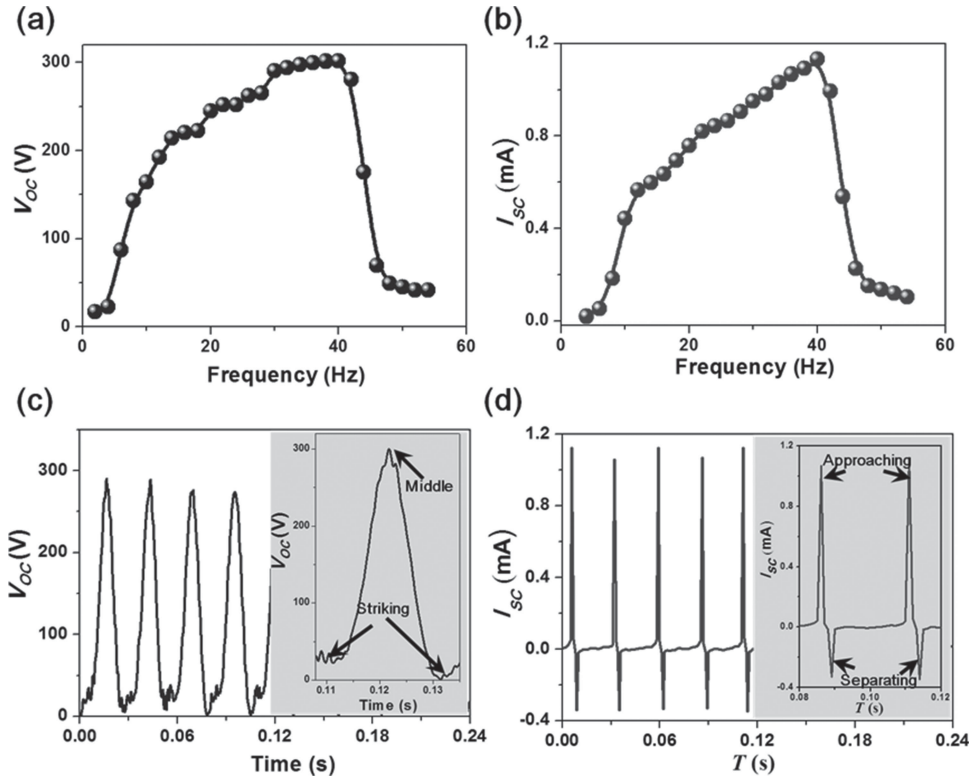


**Figure 4.** Electrical measurement results of a 3D-TENG with $n = 5$. a) Open-circuit voltage ($V_{oc}$) as a function of vibration frequency. b) Short-circuit current ($I_{sc}$) as a function of vibration frequency. c) Open-circuit voltage ($V_{oc}$) at resonant frequency of 40 Hz. Inset is an enlarged view of a cycle. d) Short-circuit current ($I_{sc}$) at resonant frequency of 40 Hz. Inset is an enlarged view of a cycle.

where $d_0$ is the thickness of PTFE, $\varepsilon_r$ is the relative permittivity of PTFE, $s$ is the effective contact area and $v$ is the relative velocity at which they will contact, whose motion direction determines the flowing direction of the induced charge, and thus the direction of the short circuit current.

Experimentally, as shown in **Figure 5**a, the voltage output is almost constant for 3D-TENG with $n = 1$–5, which is attributed to the electrically parallel connection among all the units. However, the current output is a monotonically increasing function of $n$ throughout the experimental time window. And the current enhancement factor $\alpha$ is a function of $n$, $\alpha = bn$, the measured result $b$ is very close to the ideal coefficient of 2 (Figure S5, Supporting Information). Such a high coefficient $b$ is mainly owing to the operating synchronicity of all units, which convincingly demonstrates the effectiveness of our approach for current output enhancement. Likewise, a monotonically increasing relationship was observed between the current output and the effective contact area $\Delta S$ as well as parameter $\Delta d$, as shown in Figure 5b,c. A larger $\Delta d$ will contribute to a larger relative velocity of the two contact plates, and thus renders us a higher output current, according to Equation 2. In addition, as a vibration energy harvester, we also investigate the reliance of the natural frequency on the number of pinned fingers $n$ for the 3D-TENG. As indicated in Figure 5d, the resonance frequencies $f_r$ decrease as increasing $n$, which is well consistent with a typical vibration system that a larger mass will lead to a smaller system natural frequency.[33–35]

Resistors were utilized as external loads to further investigate the output power of the 3D-TENG at its resonance frequency. As displayed in **Figure 6**a, the current amplitude drops with increasing load resistance owing to the Ohmic loss, while the voltage follows a reverse trend. Consequently, the instantaneous peak power ($P = I^2_{peak}R$) is maximized at a load resistance of 2 MΩ, coresponding to a peak power density ($P_d = I^2_{peak}R/\Delta S$) of 104.6 W m$^{-2}$ (Figure 6b). In addition, the robustness is another critical criterion for the energy harvesters. As demonstrated in Figure S6 (Supporting Information), only a slight drop of about 2% is observed for the short-circuit current after more than 1.0 million cycles of vibration.

To prove the capability of the 3D-TENG as a sustainable power source, three sets of practical applications were demonstrated. First, as shown in Figure 6c, the TENG was excited by an electrodynamic shaker at a vibration frequency of 40 Hz, lighting up a white G16 globe light (Supporting Information Movie 2). Inset is a photograph when a white G16 globe light is off. Meanwhile, a total of 20 spot lights (0.6 W ea.) connected in series were lighted up simultaneously and continuously without observable flashing. Inset is a photograph when the spot lights are off. (Figure 6d and Supporting Information Movie 3).

In addition, with specific dimensional design, we integrated a 3D-TENG into a ball with a diameter of 3 inches, as schematically shown in **Figure 7**a and a photograph of the as-fabricated devices in Figure 7b. In order to directly demonstrate the equipped ball as an energy harvester, we installed four faces

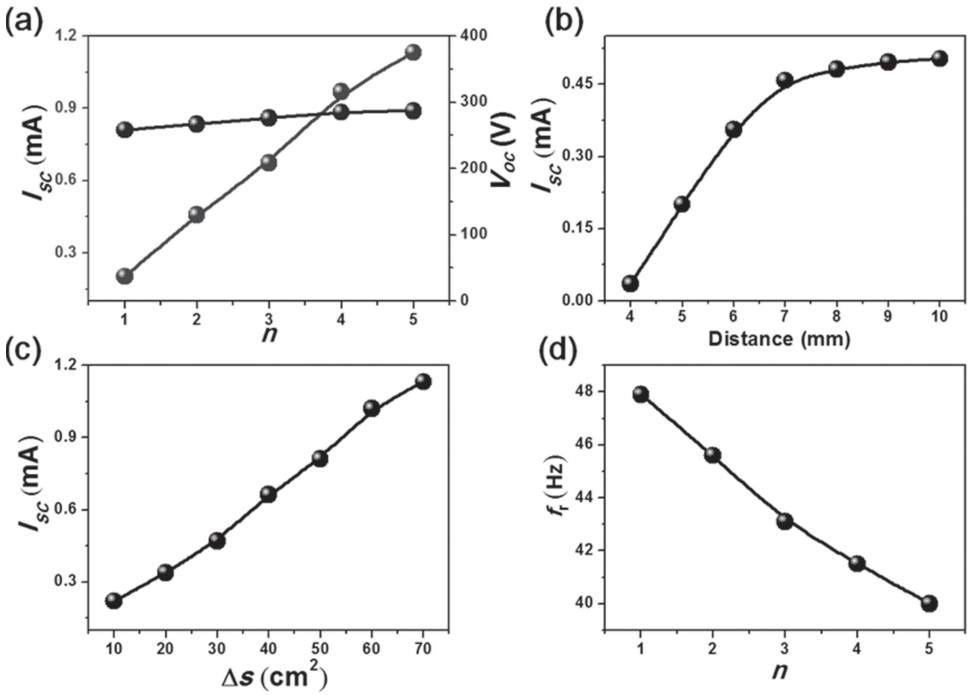


**Figure 5.** A systematical study of the reliance of current electric output on the design parameters. a) Dependence of electric output on the number of pinned fingers *n*. b) Dependence of the short-circuit current on the gap distance between two adjacent pinned fingers for the TENG with $n = 2$. c) Dependence of short-circuit current on effective contact area ($\Delta S$) of the TENG with $n = 5$. d) The device natural frequency as a function of the number of pinned fingers *n*.

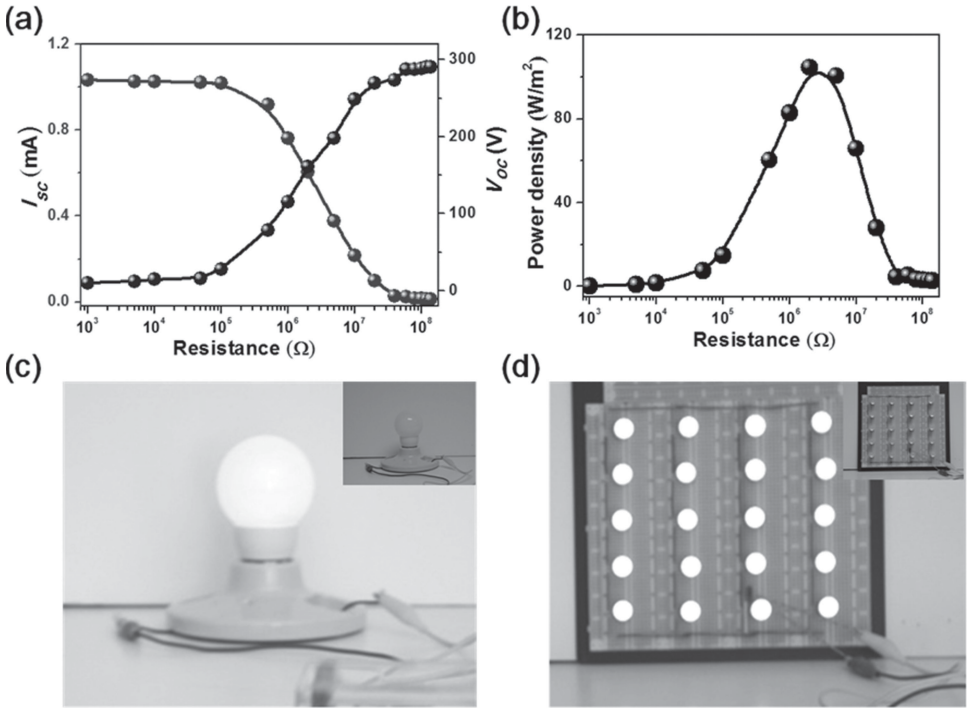


**Figure 6.** Demonstration of the 3D-TENG as a direct power source. a) Dependence of the voltage and current output on the external load resistance for the TENG with $n = 5$. The points represent peak values of electric signals while the lines are the fitted results. b) Dependence of the peak power output on the resistance of the external load for the TENG with $n = 5$, indicating maximum power output at $R = 2$ MΩ. The curve is a fitted result. c) Photograph of a white G16 globe light that is directly powered by the TENG (Input frequency 40 Hz). Inset is a photograph when a white G16 globe light is off. d) Photograph of 20 spot lights (0.6 W ea.) connected in series that are lighted up simultaneously and continuously without observable stroboflash by the TENG (Input frequency 40 Hz). Inset is a photograph when the spot lights are off.

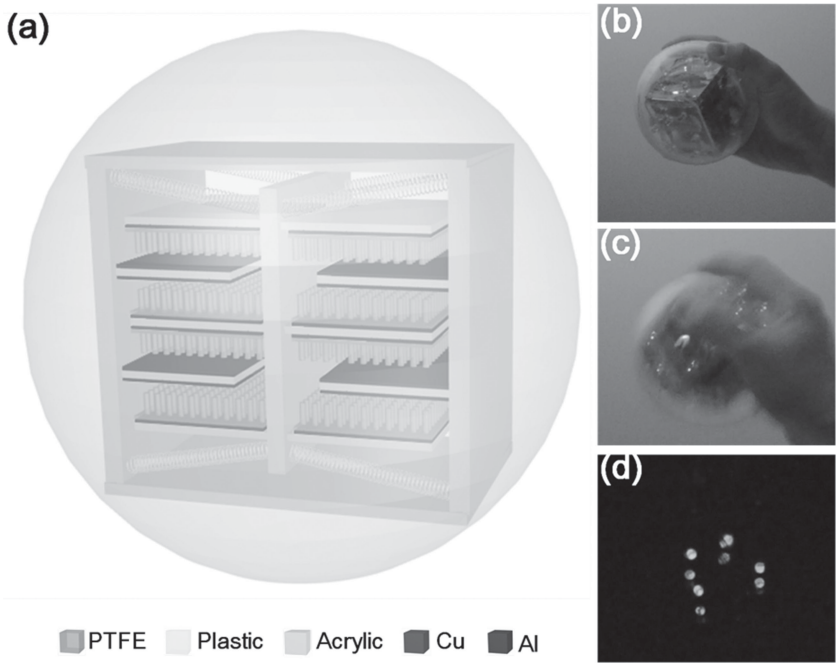


**Figure 7.** Demonstration of the 3D-TENG as it is equipped inside a ball, which has great potential of scavenging the kinetic energy when people play basketball, football, baseball and so on. Large amount of these self-powered balls can be also woven into webs for ocean wave energy harvesting, which can be potentially applied for large-scale energy generation. A sketch a) and a photograph b) of a self-powered ball. c) When shaking the ball, about 32 commercial LEDs are lighted up simultaneously. d) A photograph of 8 LEDs on a face of the device that are directly powered by the TENG in complete darkness (We equipped four faces of the devices with 8 LEDs on each face).

of the inside TENG with 8 LEDs as indicators on each face. As shown in Figure 7c, the generated power by hand shaking simultaneously lighted up 32 commercial LEDs (Supporting Information Movie 4). And Figure 7d demonstrates that 8 LEDs on one of the four faces were lighted up in complete darkness. This practical application greatly demonstrated the capability of our 3D-TENG for harvesting kinetic energy when people play various kinds of ball sports. It is worth noting that, large amount of these self-powered balls can also be woven into webs for ocean wave energy harvesting, which can be potentially applied for large-scale energy generation.

## 4. Conclusions

We have designed a 3D-TENG that is a multilayered integration of the TENGs for enhancing the output current. At the resonance frequency, it produces an open-circuit voltage of 303 V, a short-circuit current up to 1.14 mA, corresponding to a peak power density of 104.6 W $m^{-2}$. It can effectively respond to input vibration frequency from 2 Hz to 54 Hz with an extremely wide working bandwidth of 36 Hz in low frequency range. More importantly, with specific dimensional design, the 3D-TENG can be integrated into a ball with arbitary size, which can be utilized to harvest kinetic energy when people play basketball, football, baseball and so on. Ocean wave energy can also be effectively harvested by weaving large amount of these self-powered balls into webs. In a word, given its remarkable electric output power and other major advantages in weight, cost, scalability and adaptability, the TENG presented in this work is a practical approach in convertingto harvest ambient vibration energy for self-powered electronics as well as possibly for producing electricity on a large scale.

## 5. Experimental Section

*Nanowires Based PTFE Surface Modification*: A layer of 100 nm copper was firstly deposited onto the PTFE thin film with thickness of 50 μm. Then, reliance on the ICP reactive ion etching method, the aligned PTFE nanowires were created onto the copper coated PTFE surface. In the etching process, $O_2$, Ar, and $CF_4$ gases were injected into the ICP chamber with flow ratios of 10.0, 15.0, and 30.0 sccm, respectively. Plasma with a large density was generated by a power source of 400 W·A, and accelerated by another power of 100 W. The aligned PTFE nanowires were obtained after a 40-second-etching process.

*Fabrication of 3D-TENG*: Acrylic sheets with thickness of 6 mm were shaped by a laser cutter as the frameworks of our TENG. Both the pinned and movable fingers are identical to each other and made from the acrylic sheets with thickness of 3 mm with a size of 1.4 cm by 5 cm. A layer of aluminium thin film with thickness of 100 nm was deposited onto the both sides of pinned fingers as the contact electrodes by physical vapour deposition. And the as-prepared PTFE thin film with nanowires surface modification was adhered onto the movable fingers. Then, all the fingers were anchored firmly onto the framework with designed and tuneable gap distances. Lead wires were connected for electrical measurement.

## Supporting Information

Supporting Information is available from the Wiley Online Library or from the author.

## Acknowledgements

This work was supported by U.S. Department of Energy, Office of Basic Energy Sciences (Award DE-FG02–07ER46394), the "thousands talents" program for pioneer researcher and his innovation team, China, Beijing City Committee of science and technology project (Z131100006013004) and National Natural Science Foundation of China, NSFC (No. 51202023).

Received: December 18, 2013
Revised: January 14, 2014
Published online: March 24, 2014

[1] R. L. Harne, K. W. Wang, *Smart Mater. Struct.* **2013**, *22*, 023001–12.
[2] S. Roundy, P. K. Wright, J. Rabaey, *Comput. Commun.* **2003**, *26*, 1131–44.
[3] Z. L. Wang, J. H. Song, *Science* **2006**, *312*, 242.
[4] X. D. Wang, J. H. Song, J. Liu, Z. L. Wang, *Science* **2007**, *316*, 102.
[5] Y. Qin, X. Wang, Z. L. Wang, *Nature* **2008**, *451*, 809.

[6] R. S. Yang, Y. Qin, L. M. Dai, Z. L. Wang, *Nat. Nanotech.* **2008**, *4*, 34.
[7] S. P. Beeby, M. J. Tudor, N. M. White, *Meas. Sci. Technol.* **2006**, *17*, R175.
[8] S. Roundy, P. Wright, K. Pister, *Proc. IMECE* **2002**, pp 1–10.
[9] P. D. Mitcheson, E. M. Yeatman, G. Kondala Rao, A. S. Holmes, T. C. Green, *Proc. IEEE* **2008**, *96*, 1457.
[10] L. Wang, F. G. Yuan, *Smart Mater. Struct.* **2008**, *17*, 045009.
[11] I. N. Ayala-Garcia, P. D. Mitcheson, E. M. Yeatmanm, D. Zhu, J. Tudor, S. P. Beeby, *Sens. Actuators, A* **2013**, *189*, 266.
[12] Y. Wei, R. Yorah, K. Yang, S. P. Beeby, J. Tubor, *Meas. Sci. Technol.* **2013**, *24*, 075104.
[13] F.-R. Fan, Z.-Q. Tian, Z. L. Wang, *Nano Energy.* **2012**, *1*, 328.
[14] F.-R. Fan, L. Lin, G. Zhu, W. Wu, R. Zhang, Z. L. Wang, *Nano Lett.* **2012**, *12*, 3109.
[15] J. Chen, G. Zhu, W. Yang, Q. Jing, P. Bai, Y. Yang, T. C. Hou, Z. L. Wang, *Adv. Mater.* **2013**, *25*, 6094.
[16] W. Yang, J. Chen, G. Zhu, J. Yang, P. Bai, Y. Su, Q. Jing, X. Cao, Z. L. Wang, *ACS Nano* **2013**, *7*, 11317.
[17] Y. Yang, H. Zhang, J. Chen, Q. Jing, Y. Zhou, X. Wen, Z. L. Wang, *ACS Nano* **2013**, *7*, 7342.
[18] W. Yang, J. Chen, G. Zhu, X. Wen, P. Bai, Y. Su, Y. Lin, Z. L. Wang, *Nano Res.* **2013**, *6*, 880.
[19] P. Bai, G. Zhu, Y. Liu, J. Chen, Q. Jing, W. Yang, J. Ma, G. Zhang, Z. L. Wang, *ACS Nano* **2013**,*7*, 6361.
[20] J. Yang, J. Chen, Y. Yang, H. Zhang, W. Yang, P. Bai, Y. Su, Z. L. Wang, *Adv. Energy Mater.* **2013**, DOI: 10.1002/aenm.201301322.
[21] G. Zhu, J. Chen, Y. Liu, P. Bai, Y. Zhou, Q. Jing, C. Pan, Z. L. Wang, *Nano Lett.* **2013**, *13*, 2282.
[22] P. Bai, G. Zhu, Z. H. Lin, Q. Jing, J. Chen, G. Zhang, J. Ma, Z. L. Wang, *ACS Nano* **2013**, *7*, 3713.
[23] J. Lowell, A. C. Roseinnes, *Adv. Phys.* **1980**, *29*, 947.
[24] G. S. P. Castle, *J. Electrost.* **1997**, *40–1*, 13.
[25] R. G. Horn, D. T. Smith, *Science* **1992**, *256*, 362.
[26] R. G. Horn, D. T. Smith, A. Grabbe, *Nature* **1993**, *366*, 442.
[27] H. T. Baytekin, A. I. Patashinskii, M. Branicki, B. Baytekin, B.A. Grzybowski, *Science* **2011**, *333*, 308.
[28] S. Soh, S. W. Kwok, H. Liu, G.vM. Whitesides, *J. Am. Chem. Soc.* **2012**, *134*, 20151.
[29] J. A. Cross, Adam Hilger: Bristol, **1987**, Ch. 2.
[30] E. Nemeth, V. Albrecht, G. Schulert, F. Simon, *J. Electrost.* **2003**, *58*, 3.
[31] A. F. Diaz, R. M. Felix-Navarrro, *J. Electrost.* **2004**, *62*, 227.
[32] G. M. Sessler, Springer-Verlag Berlin Heidelberg: New York **1987**, Ch. 2.
[33] H. C. Liu, C. K. Lee, T. Kobayashi, C. J. Tay, C. G. Quan, *Smart Mater. Struct.* **2012**, *21*, 035005.
[34] X. Y. Wang, S. Palagummi, L. Liu, F. G. Yuan, *Smart Mater. Struct.* **2013**, *22*, 055016.
[35] K. Ashraf, M. H. M. Khir, J. O. Dennis, Z. Baharudin, *Smart Mater. Struct.* **2013**, *22*, 025018.